X-ray diffraction experiments

Henrique Teixeira
up201404859@fc.up.pt
Department of Physics and Astronomy, Faculty of Sciences of University of Porto

May 20, 2018

Abstract

This experience consisted in using x-ray diffraction with a Rigaku SmartLab Diffractometer on NaCl and W (powder and foil form), to determine this materials lattice constants and preferred orientations (when possible), using data analysis software OriginPro2017 and Excel. In this report the physical principles of relevance are explained, followed by the review of the system. The needed setup and preparations for the diffraction on the samples is also demonstrated. Later, the data collected is analyzed and discussed.
For the NaCl sample we were able to determine the lattice constant with a relative error from the tabulated value of 0.00975%, as for the W sample the preferred orientation was determined to be the (200) one and the relative errors of the lattice constants were 0.011% and 0.00126% for the powder and foil form, respectively.

Contents

I Introduction **1**

II Theoretical description and considerations **1**
i Production of X-Rays[4] 1
ii Diffraction of X-rays 2
iii Material structure influence on diffraction 3

III Rigaku Smartlab machine **3**

IV Sample preparation and machine/software setup **3**
i NaCl sample 3
ii W 4

V Results and Analysis **4**
i NaCl (Powder) 4
i.1 Theoretic Calculations . 4
i.2 Data analysis 4
ii W 7
ii.1 Theoretic Calculations (Powder) 7
ii.2 Data analysis (Powder) 7
ii.3 Data analysis (Foil) . . . 7

VI Conclusion **8**

I. Introduction

Materials are made of atoms. Knowledge of how atoms are arranged into crystal structures and microstructures is the foundation on which we build our understanding of the synthesis, structure and properties of materials. There are various techniques available to obtain this types of information about a sample, one of those is X-ray Diffraction which is considered to be one of the most accurate technique to date. In fact, most of the knowledge about the spatial arrangements of atoms in materials has been gained from diffraction experiments.

II. Theoretical description and considerations

i. Production of X-Rays[4]

Laboratory X-ray sources can be classified into two types: sealed-tube and rotating anode. Both may be used to generate monochromatic X-ray radiation and they basically differ only in the intensity of the radiation produced.

X-rays are generated when matter is irradiated by a beam of high-energy charged particles such as electrons. In the laboratory, a fila-

ment is heated to produce electrons which are then accelerated in vacuum by a high electric field in the range 20-60 kV towards a metal target, which being positive is called the anode.

When the energy of the accelerated electrons is higher than a certain threshold value (which depends on the metal anode), a second type of spectrum is obtained superimposed on top of the white radiation. It is called the characteristic radiation and is composed of discrete peaks. The energy (and wavelength) of the peaks depends solely on the metal used for the target and is due to the ejection of an electron from one of the inner electron shells of the metal atom. This results in an electron from a higher atomic level dropping to the vacant level with the emission of an X-ray photon characterized by the difference in energy between the two levels.

The characteristic lines in this type of spectrum are called K, L, M,... and they correspond to transitions to orbitals with principal quantum numbers 1, 2, 3,... When the two orbitals involved in the transition are adjacent (e.g. 2 $\rightarrow$1), the line is called α. When the two orbitals are separated by another shell (e.g. 3 $\rightarrow$ 1), the line is called β. Since the transition for β is bigger than for α, i.e. $\triangle E_\beta > \triangle E\alpha$ then $\lambda_\beta < \lambda_\alpha$.

For the copper X-Ray spectrum at high resolution the α radiation is seen as a doublet, which is labeled as $K\alpha_1$ and $K\alpha_2$ where $\Delta E\alpha_1 > \Delta E\alpha_2$. This doublets are better observed at higher diffraction angles due to the fact of both having the same wavelenght.

ii. Diffraction of X-rays

Crystalline solids consist of regular arrays of atoms, ions or molecules with interatomic spacing on the order of 100pm to 1$\AA$. When an incident X-ray reaches the surface of a material, if it has an wavelength comparable to the inter-atomic spacing, it will suffer scattering. This scattering is the result of the collision of the X-ray wave with an atom on the crystal structure which changes the wave trajectory conserving it's momentum due to the fact that the collision is elastic.

From this phenomena the diffraction of X-rays is produced and a diffraction pattern is originated from the constructive and destructive interference of the scattered waves. In a X-ray diffractometer machine, this pattern is shown as a function of intensity of number of photons scattered and the incident angle, when constructive interference is achieved it will originate a peak in the intensity otherwise the intensity will be near zero for destructive interference.

When a collimated beam of X-rays strikes a pair of parallel lattice planes in a crystal, each atom acts as a scattering center and emits a secondary wave as seen in Figure 1:

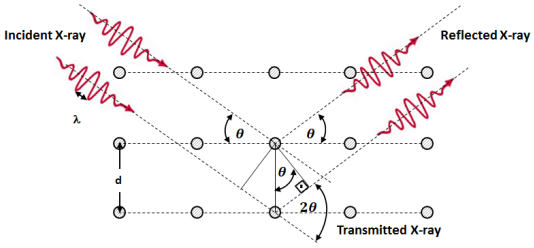

Figure 1: *Scattering of incident X-ray beam*

However the peaks in the intensity of scattered radiation will occur when rays from successive planes interfere constructively, to achieve this condition the Bragg's Law must be satisfied:

$$n\lambda = 2d_{hkl}sin\theta \tag{1}$$

This law relates the incident ray wavelength with the spacing of parallel atomic planes and the incident angle. The n variable is the order of diffraction, in X-ray diffraction experiments it's common to set n=1.

The various peaks observed in a diffraction pattern from a material correspond to different interplanar spacing. For cubic crystal systems, which are our case of interest in this report, with lattice parameter a_0, the interplanar spacing is given by:

$$d_{hkl} = \frac{a_0}{\sqrt{h^2 + k^2 + l^2}} \tag{2}$$

Where (hkl) represents the Miller indices of the material. Relating this equation with Bragg's law we see that incident angle for which intensity peaks occur is dependent on

the Miller indices, which we'll soon see depend on the sample's crystal structure. Additionally the plane normal [hkl] must be parallel to the diffraction vector to produce a peak.

iii. Material structure influence on diffraction

A given material can be classified in terms of it's crystalline structure system, being the cubic one the most simple and most common found in crystals. This crystal system is characterized by having a unit cell with the shape of a cube. The cubic crystal system can be divided in three main varieties:

- Primitive cubic
- Body-centered cubic (*BCC*)
- Face-centered cubic (*FCC*)

For each of this systems there are specific allowed Miller indices. The most basic restriction on this indices is the fact that there will be some set of them for which the sum $h^2 + k^2 + l^2$ gives no possible integral value, for example the numbers 7, 15, 23, etc. In the Primitive cubic, all are allowed with the exception of the previously discussed condition. For the two other systems the case is different, and there will be various forbidden indices. This difference arises because of the centering nature of this structures, leading to destructive interference for some reflections which are called systematic absences.

The allowed indices are able to be obtained trough the structure factor which determines the amplitude and phase of the diffracted beams:

$$F_{hkl} = \sum_{j=1}^{N} f_j e^{[-2\pi i(hx_j + ky_j + lz_j)]} \tag{3}$$

Where the sum is over all atoms in the unit cell and depends on the positional coordinates of each atom in real space and it's correspondent point in reciprocal space (hkl) and the scattering factor.

Because of the following relation: $I_{hkl} \propto |F_{hkl}|^2$, the diffraction peak intensity is determined by the arrangement of atoms in the entire crystal. So the allowed Miller indices for a given structure are the ones which satisfy the condition that the structure factor is different of zero.

III. Rigaku Smartlab machine

The Rigaku Smartlab X-Ray Diffraction machine uses a standard Copper anode sealed tube source with Tungsten filament and is capable of using Bragg-Brentano or Parallel Beam geometries for the measurements.

Figure 2: *Rigaku Smartlab X-Ray Diffraction machine*

IV. Sample preparation and machine/software setup

In this section we followed the steps explained on the document provided by the teacher, as such only the essential points of the X-ray diffractometer setup will be discussed in order to maintain this report concise.

i. NaCl sample

Preparation of sample:

The NaCl used was coarse kitchen salt which was then grounded with a mortar until a fine powder was obtained. After that an aluminum sample holder was filled with the sample powder using a glass cover-slip to homogenize the surface of the powder.[1]

This preparations were done after ensuring the machine was working as expected.

[1] In this case we need not fear of inducing a direction on the sample surface, because NaCl has a FCC crystalline structure and is highly symmetric.

Machine loading and software setup:

After having the sample holder loaded, we opened the door of the Rigaku machine and inserted it on the machine's sample plate, taking extra care to not spill the powder and assuring the sample was well centered on the plate.

Following the instructions of the provided document, we inserted the IL-slit of size 10mm. Then on the machine's software we proceed to choose our measurement package: *General (Bragg-Brentano focusing) D/teX* and perform the sample alignment using the *curved sample (Z-scan only).* Having properly aligned the sample the Kβ filter was inserted again on the machine, it's very important this filter isn't placed in it's slit during the Z-scan to avoid getting a bad sample plate position during measurement.

On the Rigaku software we choose our measurements parameters in accordance to those defined in the protocol given for this experience and then started the measurement.

ii. W

Preparation of sample (Powder/Foil):

Due to the little amount of Tungsten powder available we had to use a Silicon sample holder with a cavity in it's center. This type of sample holder is made by cutting the silicon crystal in such a way that the planes within the crystal never fulfill the Bragg condition, and they're commonly called Low-Background sample holder because of this characteristic. The big advantage of using silicon crystals in this way is that the background scatter from the mount itself is close to zero as seen in ii.2 and ii.3.

The Tungsten foil was placed on top of the sample holder, this gives a worse Z-curve producing systematic errors from the possible misplacement of the sample plate position.

Machine loading and software setup:

After loading the sample into the machine, the steps were similar to those described in i , only changing the parameters in the software for those specified in the given protocol.

V. Results and Analysis

The data from the software was given in *raw* format and converted to *xls* (Excel) using the software "*PowDLL Converter*". The wavelength of the Cu X-rays used is 1.5406 $\AA$.

i. NaCl (Powder)

i.1 Theoretic Calculations

To understand the data, we first looked upon important parameters of this sample and performed some theoretical calculations:

- Lattice constant: 5.6402 $\AA$ [1]
- Crystal Lattice type: Face-Centered-Cubic (FCC)

Using 3 the structure factor for the NaCl was calculated and the allowed Miller indices extracted:

$$F_{hkl} = \left[1 + (-1)^{h+k} + (-1)^{k+l} + (-1)^{h+l}\right]\left[f_{Na} + (-1)^h f_{Cl}\right] \tag{4}$$

With this information and with the use of equations 1, 2 and 4 a table VI was made in Excel containing the theoretic values for the diffraction angles, the inter-planar distance d_{hkl} and it's inverse squared, the allowed Miller indices for this sample and the sum of the square of each indices. The last column was added after analyzing the experimental data.[2]

i.2 Data analysis

After the measurement it's possible to see, in Figure 1, the location and shape of the region of the incident X-rays, which ionize the salt and give this particular color.

[2] All tables in this report are found in the Appendix, due to the fact of being to large to fit in a two column document.

Figure 3: *Ionizing effect of X-rays in NaCl sample*

Using OriginPro2017 we plotted the data from our measurement and also the theoretical position of the peaks from equation 1 to ease our analysis:

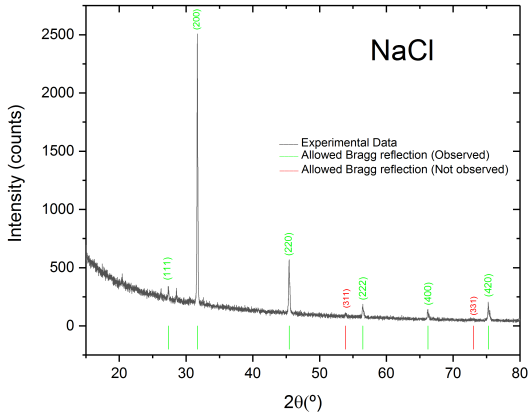

Figure 4: *NaCl Experimental Data with theoretical calculated Bragg reflections*

From analyzing Figure 4 graph it's possible to extract various relevant information. First we note that some of the theoretical calculated peaks don't appear in the experimental data, this is due to the fact that some of the crystallites are not properly oriented to diffract the X-ray beams. Also from Figure 4 we see that the most intense experimental peak corresponds to the second allowed Miller indices, the (200) plane, and not the first ones, this was expected from the structure factor for this sample, where in the (111) case we have $4(f_{Na} - f_{Cl})$ and for the (200) we have $4(f_{Na} + f_{Cl})$.

Then we used data analysis from *OriginPro 2017* software to look for the approximate location of all the peaks and then for each peak we searched the data in an interval where the peak maximum was contained and extracted the most higher value. Having now obtained the 2θ(degrees) position for each experimental peak, we used equation 2 to determine the corresponding interplanar spacing.

To obtain the Miller indices we used the following procedure:

Miller Indices calculation:

Taking equation 2, and re-arranging it to give: $\frac{1}{d_{hkl}^2} = \frac{1}{a_0^2} \times (h^2 + k^2 + l^2)$. We see that all the inverse squared interplanar spacing of the peaks will have a common factor, which is the inverse square of the lattice constant. So if we find the second term of the right side of this equation for the first peak we know our first Miller indices.

So the procedure is as follows:

1. Find the integer which multiplied by $\frac{1}{a_0^2}$ gives $\frac{1}{d_{hkl}^2}$ of the first peak, obtaining then the Miller indices of this peak;
2. Set $Z = \frac{1}{d_1^2 \times n_1}$, where d_1 is the interplanar distance and n_1 are the squared sum of the Miller indices of the first peak;
3. Do $\frac{\frac{1}{d_2^2}}{Z} = \frac{n_2}{n_1} \times n_1 = n_2$
4. Repeat for the following peaks

With all this information gathered it was possible to build a table VI containing all the experimental peaks with the corresponding incident angles, interplanar distance and it's relative error, the Miller indices, lattice constant and it's relative error and finally the ordering of the peaks intensity. It was also possible to observe two peaks of the second order which are identified on the table.

Looking with more attention to the graphic of Figure 4 we notice that the peaks corresponding to higher diffraction angles have a distinct adjacent peak which is also a little shorter. This was expected from the theory

discussed in i. Even though we filter the $K\beta$ radiation, the Rigaku machine dos note filter $K\alpha$ radiation, and as such instead of only having the desired $K\alpha_1$ X-rays beams colliding with the sample we have also the $K\alpha_2$ ones. In Figure 5 we can observe (zoomed) the expected effects of this radiation, comparing it's intensities and angle displacement for low diffraction angles and high ones:

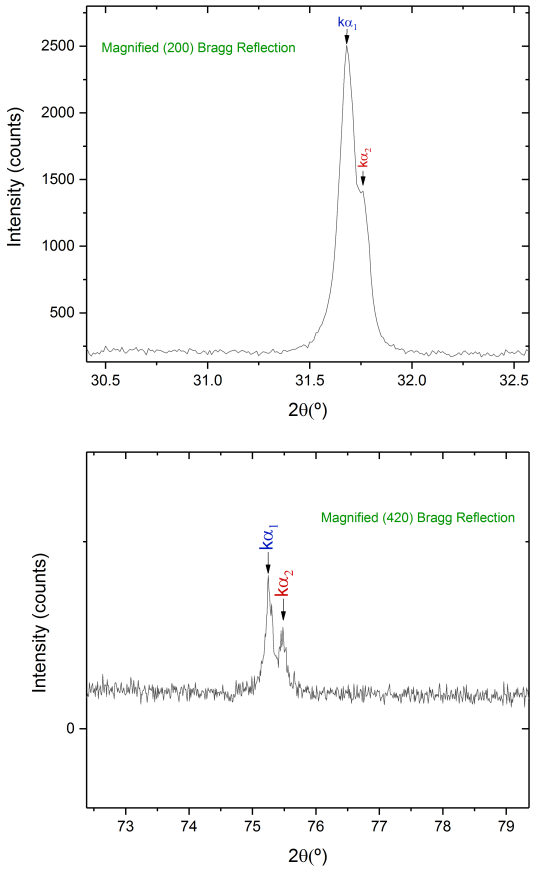

Figure 5: *Comparison of low and high diffraction angles*

Having analyzed all this information the only thing left was to obtain a final experimental value for the lattice parameter. For this sample we have calculated six different values, but which do we choose ? Next we explain how we reached the final value for this sample lattice parameter:

Lattice Parameter Extrapolation:

With a powder diffractometer it is possible to measure lattice parameters to an accuracy of better than 1 part in 10,000. This accuracy cannot be achieved, however, by simply applying Bragg's law to one peak in a diffraction pattern, owing to several practical problems. The most serious is that the center of diffraction is not located precisely at the center of the goniometer. This is caused by inaccurate sample positioning, irregularities of the specimen surface, and, more subtly, by variations in the x-ray penetration depth for different materials.

As such by differentiating the errors associated with sample bad position within the plate, angle and interplanar distance we reach a linear expression for the Bragg-Brentano geometry for our lattice parameter error[3]:

$$a = a_0 + a_0 K' \left(\frac{cos^2\theta}{sin\theta} \right) \tag{5}$$

where $K' = \triangle y / (R sin\, w)$ is a constant, θ is the experimental value of the diffraction angles, a_0 is the true estimation of the lattice parameter and a is the apparent lattice parameter calculated from the angular position of a particular (hkl) diffraction peak.

Equation 5 implies that the actual lattice parameter a_0 is obtained by plotting each experimental calculated a value with respect to $\left(\frac{cos^2\theta}{sin\theta} \right)$, extrapolating it to $\left(\frac{cos^2\theta}{sin\theta} \right) = 0$.

As such, using *OriginPro 2017* to plot this values and then performing a linear fit using a least-squares fitting algorithm we get the following graph:

[3]For more information about this equation see [2]

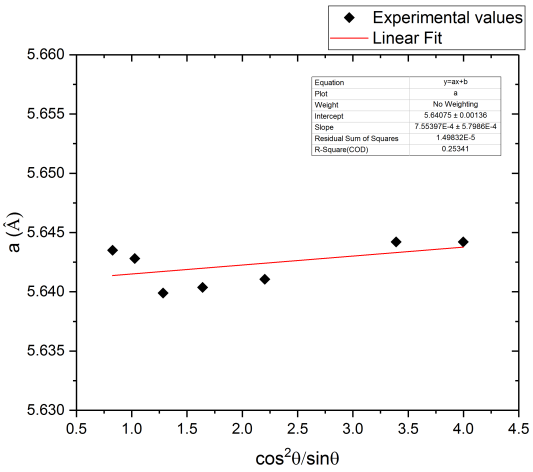

Figure 6: *NaCl Lattice Parameter Extrapolation*

and a linear relationship was obtained between a_0 and x:

$$a = 5.64075 + (7.55397E - 4)x \qquad (6)$$

Obtaining than a value of the lattice parameter for the NaCl with a resolution within $\frac{1}{10}$ of a picometer:

$$a_0 = (5.64075 \pm 0.00136)\mathring{A} \qquad (7)$$

Giving a relative error compared to the tabulated value of 0.00975%.

ii. W

ii.1 Theoretic Calculations (Powder)

Tabulated parameters:

- Lattice constant: 3.1652 $\mathring{A}$ [3]
- Crystal Lattice type: Body-Centered-Cubic (BCC)

Using 3 the structure factor for Tungsten is given by:

$$F_{hkl} = \left[1 + (-1)^{h+k+l}\right][f_W] \qquad (8)$$

Similar to i.1, a theoretical table was also made VI.

ii.2 Data analysis (Powder)

Plotting the graph for this sample we notice right away the influence that the Low-Background sample holder has, removing all background noise associated with the material it's made by:

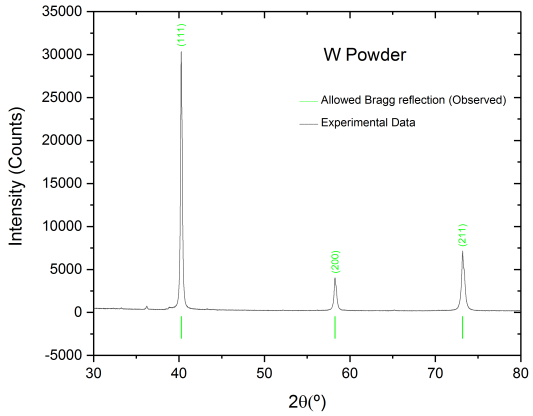

Figure 7: *W(Powder) Experimental Data with theoretical calculated Bragg reflections*

We also constructed a table VI with the experimental values analogous to the one from the NaCl sample.

The extrapolated lattice parameter was obtained as explained in i.2 :

$$a_0 = (3.16485 \pm 2.13628E - 4)\mathring{A} \qquad (9)$$

With a relative error of 0.011%.

ii.3 Data analysis (Foil)

For this form of Tungsten, the intensity peaks have much higher values:

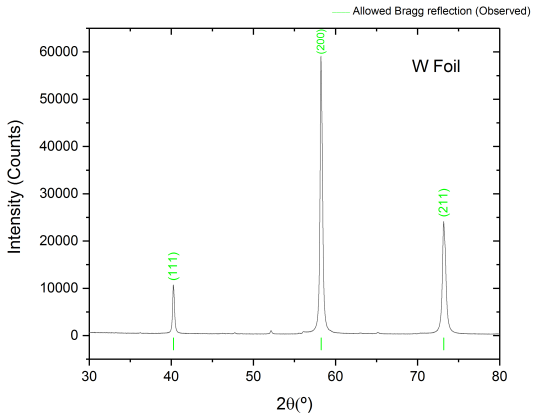

Figure 8: *W(Foil) Experimental Data with theoretical calculated Bragg reflections*

this was expected because this state is anisotropic and as such the direction of the crystal planes is being privileged, contrary from at is happening at ii.2, where the sample is isotropic meaning that all the planes have equally probability of reflecting the X-rays.

For a better analysis of the two states of W, the following graph was made:

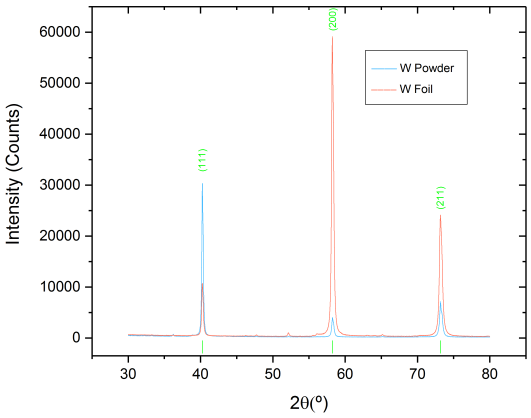

Figure 9: *W state's comparison*

Where we see the difference in the intensities and note that both states have the same number of peaks due to the fact of W being a monocrystal and it's structure is cubic.

It's easy to notice also that the preferred orientation of the Tungsten foil is the (200) plane.

The extrapolated lattice parameter of the W foil is:

$$a_0 = (3.16524 \pm 8.97407E-4)\mathring{A} \qquad (10)$$

With a relative error of 0.00126%. A much lesser error than the powder form, giving us a precision on order bellow of the fentometer scale.

VI. Conclusion

With this experiment, using a Rigaku SmartLab X-ray Diffractometer, we were able to study the crystal structure of two different materials, obtaining the lattice constant's with very high precision. It was also possible to study the effects of anisotropy on a Tungsten sample. The value of the calculated experimental lattice constant could be improved by using the Rietveld method[5].

This experiment shows that X-Ray Diffraction is a powerful tool to analyse various types of substance.

References

[1] W. T. Barrett and W. E. Wallace. Studies of nacl-kcl solid solutions. i. heats of formation, lattice spacings, densities, schottky defects and mutual solubilities1,2. *Journal of the American Chemical Society*, 76(2):366–369, 1954.

[2] B.D. Cullity. *Elements of X-ray Diffraction*. Addison-Wesley series in metallurgy and materials. Addison-Wesley Publishing Company, 1978.

[3] W. P. Davey. Precision Measurements of the Lattice Constants of Twelve Common Metals. *Physical Review*, 25:753–761, June 1925.

[4] R.E. Dinnebier and S.J.L. Billinge. *Powder Diffraction: Theory and Practice*. Royal Society of Chemistry, 2008.

[5] H. P. Klug and L. E. Alexander. *X-Ray Diffraction Procedures: For Polycrystalline and Amorphous Materials, 2nd Edition*. May 1974.

Appendix

Theoretical tables:

Peak	2θ(°)	θ(°)	d (Å)	1/d^2	h²+k²+l²	h	k	l	a (Å)	Observed peaks
1	27.36621231	13.6831	3.25637	0.0943	3	1	1	1	5.6402	✓
2	31.70315736	15.8516	2.8201	0.12574	4	2	0	0	5.6402	✓
3	45.44735665	22.7237	1.99411	0.25148	8	2	2	0	5.6402	✓
4	53.86775993	26.9339	1.70058	0.34578	11	3	1	1	5.6402	✗
5	56.47186108	28.2359	1.62819	0.37722	12	2	2	2	5.6402	✓
6	66.22609103	33.113	1.41005	0.50296	16	4	0	0	5.6402	✓
7	73.06927659	36.5346	1.29395	0.59726	19	3	3	1	5.6402	✗
8	75.29094804	37.6455	1.26119	0.6287	20	4	2	0	5.6402	✓

Table 1: *NaCl*

Peak	2θ(°)	θ(°)	d (Å)	1/d^2	h²+k²+l²	h	k	l	a (Å)	Observed peaks
1	40.2623	20.1312	2.23813	0.19963	2	1	1	0	3.1652	✓
2	58.2519	29.1259	1.5826	0.39926	4	2	0	0	3.1652	✓
3	73.1852	36.5926	1.29219	0.59889	6	2	1	1	3.1652	✓

Table 2: *W (Powder)*

Peak	2θ(°)	θ(°)	d (Å)	1/d^2	h²+k²+l²	h	k	l	a (Å)	Observed peaks
1	40.2623	20.1312	2.23813	0.199630862	2	1	1	0	3.1652	✓
2	58.2519	29.1259	1.5826	0.399261724	4	2	0	0	3.1652	✓
3	73.1852	36.5926	1.29219	0.598892585	6	2	1	1	3.1652	✓

Table 3: *W(Foil)*

Experimental tables:

Peak	2θ(°)	θ(°)	d (Å)	d - relative error (%)	1/d^2	(1/d^2)/Z	h²+k²+l² ((1/d^2)/Z)	h	k	l	Diffraction order	a (Å)	a - relative error (%)	Intensity order (highest to low)
1	27.32	13.66	3.261774178	0.16592672	0.093992	3	3	1	1	1	1º	5.649558599	0.16592672	3
2	31.69	15.845	2.821240855	0.040454425	0.125638	4.010040017	4	2	0	0	1º	5.64248171	0.040454425	1
3	45.44	22.72	1.994417571	0.015332	0.251401	8.024109599	8	2	2	0	1º	5.641064755	0.015332	2
4	56.47	28.235	1.628234738	0.003024484	0.377195	12.0391272	12	2	2	2	2ª	5.640370587	0.003024484	5
5	66.23	33.115	1.409976256	0.005229869	0.50301	16.05481985	16	4	0	0	2ª	5.639905025	0.005229869	6
6	75.25	37.625	1.261771661	0.046353175	0.628114	20.04783583	20	4	2	0	1º	5.642814412	0.046353175	4

Table 4: *NaCl*

Peak	2θ(°)	θ(°)	d (Å)	d - relative error (%)	1/d^2	(1/d^2)/Z	h²+k²+l² (round left cell)	h	k	l	a (Å)	a - relative error (%)	Intensity order (highest to low)
1	40.26	20.13	2.23826	0.00558473	0.19961	2	2	1	1	1	3.16538	0.00558473	1
2	58.25	29.125	1.58265	0.002898432	0.39924	4.0002149	4	2	0	0	3.16529	0.002898432	3
3	73.19	36.595	1.29211	0.005684695	0.59896	6.001352483	6	2	1	1	3.16502	0.005684695	2

Table 5: *W (Powder)*

Peak	2θ(°)	θ(°)	d (Å)	d - relative error (%)	1/d^2	(1/d^2)/Z	h²+k²+l² (round left cell)	h	k	l	a (Å)	a - relative error (%)	Intensity order (highest to low)
1	40.25	20.125	2.23879	0.029400159	0.19951	1.999047776	2	1	1	1	3.16613	0.029400159	3
2	58.23	29.115	1.58314	0.034235886	0.39899	3.997709019	4	2	0	0	3.16628	0.034235886	1
3	73.18	36.59	1.29227	0.00606898	0.59882	5.999941892	6	2	1	1	3.16539	0.00606898	2

Table 6: *W (Foil)*